Pulsating flow of an incompressible micropolar fluid between permeable beds

Article *in* Nonlinear Analysis Modelling and Control · September 2013

DOI: 10.15388/NA.18.4.13969

2 authors:

Bitla Punnamchandar
Tripura University
15 PUBLICATIONS **88** CITATIONS
SEE PROFILE

T.K.V. Iyengar
National Institute of Technology, Warangal
38 PUBLICATIONS **479** CITATIONS
SEE PROFILE

Pulsating flow of an incompressible micropolar fluid between permeable beds

Punnamchandar Bitla, Telikicherla Kandala Venkatacharyulu Iyengar

Department of Mathematics, National Institute of Technology
Warangal-506004, Andhra Pradesh, India
punnam.nitw@gmail.com; iyengar.tkv@gmail.com

Received: 13 December 2011 / **Revised:** 6 June 2013 / **Published online:** 25 September 2013

Abstract. The paper deals with the pulsating flow of an incompressible micropolar fluid through a channel bounded by permeable beds. The fluid is injected into the channel from the lower permeable bed with a certain velocity and is sucked into the upper permeable bed with the same velocity. The flow between the permeable beds is assumed to be governed by micropolar fluid flow equations and that in the permeable regions by Darcy law. The Beavers–Joseph (BJ) slip boundary conditions are used at the interfaces of the permeable beds. The governing equations are solved analytically and the expressions for velocity, microrotation, mass flux and shear stress are obtained. The effects of diverse parameters on the velocity and microrotation are studied numerically and the results are presented through graphs.

Keywords: pulsating flow, micropolar fluid, microrotation, Darcy law, BJ condition, permeable beds, shear stress.

1 Introduction

Pulsating flow is a special kind of unsteady flow in which a periodic variation in flow velocity is superimposed on steady velocity. The accurate measurement of pulsating velocity is of great importance in many industrial and medical applications. Pulsating flow is frequently encountered in natural systems (human respiratory, circulatory and vascular systems) [1, 2] and engineering systems (exhaust and intake manifolds of internal combustion engines, thermoacoustic coolers, Stirling engines, etc.) [3]. Pulsatile flow has also recently found renewed significance in its application to MEMS microfluidic engineering applications [4]. A complete treatment of the fluid dynamics of steady and pulsatory flow with emphasis on basic mechanics, physics and applications can be seen [5]. A critical account on pulsatile pipe flow studies directing towards future research topics has been presented by Carpinlioglu and Gundogdu [6].

It can be noticed that the flow through porous media has attracted considerable research activity in recent years because of its several important applications notably in the flow of oil through porous rock, the extraction of energy from the geothermal regions,

the evaluation of the capability of heat-removal from particulate nuclear fuel debris that may result from a hypothetical accident in a nuclear reactor, the filteration of solids from liquids, flow of ion-exchange beds, drug permeation through human skin, chemical reactors for economical separation or purification of mixtures and so on [7–9]. In the case of flow past porous medium, Beavers and Joseph [10] have shown that the usual no-slip condition at the porous boundaries is no longer valid and they have postulated the existance of a slip at the interface of a permeable boundary resulting in the condition called BJ slip condition. According to this condition, the Poiseuille velocity in the channel and the Darcy's velocity in the porous wall can be coupled through the following equation:

$$\left(\frac{\mathrm{d}u}{\mathrm{d}y}\right)_{y=0+} = \frac{\alpha}{\sqrt{k}}(u_s - u_D).$$

Here $u_s = u|_{y=0+}$ is the slip velocity, i.e., the local averaged tangential velocity just outside the porous medium, u_D $(= -(k/\mu)\partial p/\partial x)$ is the velocity inside the porous bed, given by Darcy's law, k is the permeability of the porous medium and the slip coefficient α is a dimensionless constant which is independent of the viscosity of the fluid, but dependent on the material parameters that characterize the structure of the permeable material within the boundary region. It has been shown that the value of α depends on the flow direction at the interface, the Reynolds number, the extent of the clear fluid, and the non-uniformities in the arrangement of solid material at the surface [11].

Verma et al. [12] studied the pulsatile blood flow of a microdeformable fluid. A mathematical model for the study of blood flow through a channel with permeable walls of finite width is discussed by Mishra and Ghosh [13]. Vajravelu et al. [14] studied the pulsatile flow of a viscous incompressible Newtonian fluid between permeable beds. Lalit and Narayanan [15] discussed the analysis of pulsatile flow and its role on particle removal from surfaces.

To the extent the present authors have surveyed the pulsatile flow of an incompressible micropolar fluid between two permeable beds has not been studied so far. The micropolar fluid dynamics introduced by Eringen [16, 17] exhibits some microscopic effects arising from the local structure and micro motion of the fluid elements. *It is distinguished from the classical fluid dynamics (which is also known as Newtonian fluid dynamics or Navier-Stokes(N-S) theory) in that classical fluid dynamics is assumed not to possess oriented material points. Thus, against the three translational degrees of freedom of the classical theory, micropolar fluid theory accounts for six degrees of freedom: three translational degrees and three rotational degrees. The rotational degrees of freedom bring into play nonsymmetric stress tensors and couple stresses, which are missing from the classical theory* [18]. Micropolar fluids have been shown to accurately simulate the flow characteristics of polymeric additives, geomorphological sediments, colloidal suspensions, haematological suspensions, liquid crystals, lubricants etc. The mathematical theory of equations of micropolar fluids and applications of these fluids in the theory of lubrication and porous media are presented succinctly by Lukaszewicz [19].

In this paper we have chosen to study the flow of an incompressible micropolar fluid between permeable beds, because of its importance in many industrial problems and its

relevance to diverse natural phenomena. The flow is assumed to be driven by an unsteady pulsating pressure gradient. The flow through the permeable beds is assumed to be governed by Darcy's law and the flow between the permeable beds by Eringen's micropolar fluid flow equations. Following [10, 11], herein we have adopted the Beavers–Joseph (BJ) slip boundary conditions at the interfaces of the permeable beds. The equations are solved analytically and the expressions for velocity, microrotation and mass flux are obtained. The effects of the pertinent parameters on the velocity and microrotation are studied numerically and the results are presented through graphs.

2 Mathematical formulation

A physical model illustrating the problem under consideration is shown in Fig. 1 which consists of an infinite channel bounded by permeable beds. Let the x-axis be taken along the interface of the lower permeable bed and the y-axis perpendicular to it. Let $y = 0$ and $y = h$ represent the interfaces of the permeable beds. We consider the unsteady, laminar, incompressible pulsating flow of a micropolar fluid between two permeable beds. The fluid is injected into the channel from the lower permeable bed with a velocity U and is sucked into the upper permeable bed with the same velocity. The permeabilities of lower and upper beds are k_1 and k_2, respectively. It is assumed that the permeable beds are rigid, homogeneous and isotropic. The flow in upper and lower permeable beds is assumed to be governed by Darcy's law. The flow between the permeable beds is assumed to be governed by micropolar fluid flow equations.

The field equations describing a micropolar fluid [17] flow are given by

$$\frac{\partial \rho}{\partial t} + \operatorname{div}(\rho \vec{V}) = 0, \tag{1}$$

$$\rho \frac{\mathrm{d}\vec{V}}{\mathrm{d}t} = \rho \vec{f} - \operatorname{grad} p + \kappa \operatorname{curl} \vec{\nu} - (\mu + \kappa) \operatorname{curl}(\operatorname{curl} \vec{V}) + (\lambda + 2\mu + \kappa) \operatorname{grad}(\operatorname{div} \vec{V}), \tag{2}$$

$$\rho j \frac{\mathrm{d}\vec{\nu}}{\mathrm{d}t} = \rho \vec{l} - 2\kappa \vec{\nu} + \kappa \operatorname{curl} \vec{V} - \gamma \operatorname{curl}(\operatorname{curl} \vec{\nu}) + (\alpha_1 + \beta + \gamma) \operatorname{grad}(\operatorname{div} \vec{\nu}), \tag{3}$$

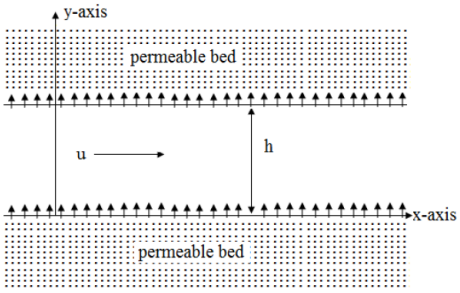

Fig. 1. Flow diagram.

where $\vec{V}$ and $\vec{\nu}$ are velocity and microrotation vectors, respectively. $\vec{f}$, $\vec{l}$ are the body force per unit mass and body couple per unit mass, respectively, and p is the pressure at any point. ρ and j are the density of the fluid and gyration parameter, respectively, and are assumed to be constant. The material quantities (λ, μ, κ) are viscosity coefficients and (α_1, β, γ) are gyroviscosity coefficients satisfying the constraints

$$\begin{aligned} &\kappa \geqslant 0, \qquad 2\mu + \kappa \geqslant 0, \qquad 3\lambda + 2\mu + \kappa \geqslant 0, \\ &\gamma \geqslant 0, \qquad \beta \geqslant \gamma, \qquad 3\alpha_1 + \beta + \gamma \geqslant 0. \end{aligned}$$

Equations (1)–(3) represent the conservation of mass, conservation of linear momentum and conservation of micro-inertia, respectively. In the absence of $\vec{l}$, $\vec{f}$ and $\kappa = \alpha_1 = \beta = \gamma = 0$, microrotation (gyration) vector becomes zero and the governing equations reduce to Navier–Stokes equations.

It is assumed that the flow is laminar and fully developed and is driven by pulsating pressure gradient,

$$-\frac{\partial p}{\partial x} = \left(\frac{\partial p}{\partial x}\right)_{\mathrm{s}} + \left(\frac{\partial p}{\partial x}\right)_{\mathrm{o}} \mathrm{e}^{\mathrm{i}\omega t},$$

where $(\partial p/\partial x)_{\mathrm{s}}$ and $(\partial p/\partial x)_{\mathrm{o}}$ are amplitudes of steady and oscillatory pulsations, respectively, and ω is the frequency. It is further assumed that the thickness of the permeable beds is much larger than the width of the channel so that we can directly use Beavers–Joseph condition at the interfaces of the channel. Under the assumptions made, we have $\vec{V} = (u(y,t), U, 0)$ and $\vec{\nu} = (0, 0, c(y,t))$. In the absence of body forces and body couples, the governing fluid flow equations of the problem are given by

$$\begin{aligned} &\rho\left(\frac{\partial u}{\partial t} + U\frac{\partial u}{\partial y}\right) = -\frac{\partial p}{\partial x} + \kappa\frac{\partial c}{\partial y} + (\mu + \kappa)\frac{\partial^2 u}{\partial y^2}, \\ &\rho j\left(\frac{\partial c}{\partial t} + U\frac{\partial c}{\partial y}\right) = -2\kappa c - \kappa\frac{\partial u}{\partial y} + \gamma\frac{\partial^2 c}{\partial y^2}. \end{aligned}$$

Herein the velocity component $u(y,t)$ is to satisfy the conditions

$$\begin{aligned} &\frac{\partial u}{\partial y} = \frac{\alpha}{\sqrt{k_1}}(u_{B_1} - Q_1) \quad \text{at } y = 0, \\ &\frac{\partial u}{\partial y} = -\frac{\alpha}{\sqrt{k_2}}(u_{B_2} - Q_2) \quad \text{at } y = h, \end{aligned} \tag{4}$$

and the microrotation component $c(y,t)$ is to satisfy the condition

$$c = 0 \quad \text{at } y = 0 \text{ and } y = h, \tag{5}$$

where $u_{B_1} = u|_{y=0}$ and $u_{B_2} = u|_{y=h}$ are the slip velocities at the interfaces of the lower and upper permeable beds, respectively. α is the slip parameter. $Q_1 = -(k_1/\mu)\partial p/\partial x$ and $Q_2 = -(k_2/\mu)\partial p/\partial x$ are Darcy's velocities in the lower and upper permeable beds, respectively. Equation (4) represents the BJ slip boundary conditions respectively,

at the interfaces of the lower and upper permeable beds. Equation (5) stipulates that the microrotation vanishes at the interfaces of the permeable beds.

In view of the pulsating pressure gradient, let us assume that the velocity and microrotation are in the form

$$u = u_{\mathrm{s}} + u_{\mathrm{o}}\mathrm{e}^{\mathrm{i}\omega t}, \qquad c = c_{\mathrm{s}} + c_{\mathrm{o}}\mathrm{e}^{\mathrm{i}\omega t}.$$

where u_{s} and c_{s} represent steady parts and u_{o} and c_{o} represent the oscillatory parts of the velocity and microrotation, respectively.

3 Non-dimensionalization of the flow quantities

The following non-dimensional quantities are introduced to make the governing equations and the boundary conditions dimensionless:

$$\begin{aligned}
&u^* = \frac{u}{U}, \qquad {u_{\mathrm{s}}}^* = \frac{u_{\mathrm{s}}}{U}, \qquad {u_{\mathrm{o}}}^* = \frac{u_{\mathrm{o}}}{U}, \qquad c^* = \frac{ch}{U},\\
&c_{\mathrm{s}}^* = \frac{c_s h}{U}, \qquad {c_{\mathrm{o}}}^* = \frac{c_o h}{U}, \qquad u_{B_1}^* = \frac{u_{B_1}}{U}, \qquad u_{B_2}^* = \frac{u_{B_2}}{U},\\
&p^* = \frac{p}{\rho U^2}, \qquad \omega^* = \frac{\omega h}{U}, \qquad t^* = \frac{tV}{h}, \qquad x^* = \frac{x}{h}, \qquad y^* = \frac{y}{h}.
\end{aligned}$$

The equations and boundary conditions governing the non-dimensionalized pulsatile flow are given by

$$\begin{aligned}
&\frac{\partial^2 u}{\partial y^2} + m\frac{\partial c}{\partial y} - R\left(\frac{\partial u}{\partial y} + \frac{\partial u}{\partial t}\right) = R\left(\frac{\partial p}{\partial x}\right),\\
&\frac{\partial^2 c}{\partial y^2} - n\frac{\partial u}{\partial y} - RP_j\left(\frac{\partial c}{\partial y} + \frac{\partial c}{\partial t}\right) - 2nc = 0,
\end{aligned}$$

after dropping $*$'s.

The non-dimensionalized boundary conditions on u and c are

$$\begin{aligned}
&\frac{du}{dy} = \alpha\sigma_1\left(u_{B_1} - \frac{R}{(1-m)\sigma_1^2}\frac{\partial p}{\partial x}\right) \quad \text{at } y = 0,\\
&\frac{du}{dy} = -\alpha\sigma_2\left(u_{B_2} - \frac{R}{(1-m)\sigma_2^2}\frac{\partial p}{\partial x}\right) \quad \text{at } y = 1,\\
&c = 0 \quad \text{at } y = 0 \text{ and } 1,
\end{aligned}$$

where

$$\begin{aligned}
&u = u_{\mathrm{s}} + u_{\mathrm{o}}\mathrm{e}^{\mathrm{i}\omega t}, \qquad c = c_{\mathrm{s}} + c_{\mathrm{o}}\mathrm{e}^{\mathrm{i}\omega t},\\
&-\frac{\partial p}{\partial x} = \left(\frac{\partial p}{\partial x}\right)_{\mathrm{s}} + \left(\frac{\partial p}{\partial x}\right)_{\mathrm{o}}\mathrm{e}^{\mathrm{i}\omega t},\\
&u_{B_1} = u_{s_{B1}} + u_{o_{B1}}\mathrm{e}^{\mathrm{i}\omega t}, \qquad u_{B_2} = u_{s_{B2}} + u_{o_{B2}}\mathrm{e}^{\mathrm{i}\omega t}.
\end{aligned}$$

Reynolds number $R = (\rho U h)/(\mu + \kappa)$, coupling parameter $m = \kappa/(\mu + \kappa)$, gyration parameter $n = \kappa h^2/\gamma$, microrotation parameter $P_j = j(\mu + \kappa)/\gamma$, $\sigma_1 = h/\sqrt{k_1}$ and $\sigma_2 = h/\sqrt{k_2}$ are non-dimensional parameters inversely proportional to the square root of the permeabilities of the lower and upper permeable beds, respectively.

3.1 Steady flow

The governing equations of steady flow are given by

$$\frac{\partial^2 u_{\rm s}}{\partial y^2} + m\frac{\partial c_{\rm s}}{\partial y} - R\frac{\partial u_{\rm s}}{\partial y} = -RP_{\rm s},$$
$$\frac{\partial^2 c_{\rm s}}{\partial y^2} - n\frac{\partial u_{\rm s}}{\partial y} - RP_j\frac{\partial c_{\rm s}}{\partial y} - 2nc_{\rm s} = 0.$$

The boundary conditions to be satisfied by $u_{\rm s}$ and$c_{\rm s}$ are

$$\frac{{\rm d}u_{\rm s}}{{\rm d}y} = \alpha\sigma_1\left(u_{sB_1} - \frac{RP_{\rm s}}{(1-m)\sigma_1^2}\right) \quad \text{at } y = 0,$$
$$\frac{{\rm d}u_{\rm s}}{{\rm d}y} = -\alpha\sigma_2\left(u_{sB_2} - \frac{RP_{\rm s}}{(1-m)\sigma_2^2}\right) \quad \text{at } y = 1,$$
$$c_{\rm s} = 0 \quad \text{at } y = 0 \text{ and } 1,$$

where $P_{\rm s} = (\partial p/\partial x)_{\rm s}$.

3.2 Oscillatory flow

The governing equations of oscillatory flow are given by

$$\frac{\partial^2 u_{\rm o}}{\partial y^2} + m\frac{\partial c_{\rm o}}{\partial y} - R\frac{\partial u_{\rm o}}{\partial y} - {\rm i}\omega R u_{\rm o} = -RP_{\rm o},$$
$$\frac{\partial^2 c_{\rm o}}{\partial y^2} - n\frac{\partial u_{\rm o}}{\partial y} - RP_j\frac{\partial c_{\rm o}}{\partial y} - (2n + {\rm i}\omega RP_j)c_{\rm o} = 0.$$

The boundary conditions to be satisfied by $u_{\rm o}$ and$c_{\rm o}$ are

$$\frac{{\rm d}u_{\rm o}}{{\rm d}y} = \alpha\sigma_1\left(u_{oB_1} - \frac{RP_{\rm o}}{(1-m)\sigma_1^2}\right) \quad \text{at } y = 0,$$
$$\frac{{\rm d}u_{\rm o}}{{\rm d}y} = -\alpha\sigma_2\left(u_{oB_2} - \frac{RP_{\rm o}}{(1-m)\sigma_2^2}\right) \quad \text{at } y = 1,$$
$$c_{\rm o} = 0 \quad \text{at } y = 0 \text{ and } 1,$$

where $P_{\rm o} = (\partial p/\partial x)_{\rm o}$.

4 Solution of the problem

4.1 Steady flow solution

The solution of the steady flow described in Section 3.1 is given by

$$u_{\mathrm{s}} = C_1 + P_s y + C_2 \mathrm{e}^{\lambda_2 y} + C_3 \mathrm{e}^{\lambda_3 y} + C_4 \mathrm{e}^{\lambda_4 y}, \tag{6}$$

$$c_{\mathrm{s}} = D_2 \mathrm{e}^{\lambda_2 y} + D_3 \mathrm{e}^{\lambda_3 y} + D_4 \mathrm{e}^{\lambda_4 y} - \frac{P_{\mathrm{s}}}{2}, \tag{7}$$

where C_j, $j = 1, 2, 3, 4$, D_j, $j = 2, 3, 4$, and λ_j, $j = 2, 3, 4$, are not reported for brevity.

4.2 Oscillatory flow solution

The solution of the oscillatory flow described in Section 3.2 is given by

$$u_{\mathrm{o}} = C_5 \mathrm{e}^{\lambda_5 y} + C_6 \mathrm{e}^{\lambda_6 y} + C_7 \mathrm{e}^{\lambda_7 y} + C_8 \mathrm{e}^{\lambda_8 y} - \frac{\mathrm{i} P_{\mathrm{o}}}{\omega}, \tag{8}$$

$$c_{\mathrm{o}} = D_5 \mathrm{e}^{\lambda_5 y} + D_6 \mathrm{e}^{\lambda_6 y} + D_7 \mathrm{e}^{\lambda_7 y} + D_8 \mathrm{e}^{\lambda_8 y}, \tag{9}$$

where C_j, $j = 5, 6, 7, 8$, D_j, $j = 5, 6, 7, 8$, and λ_j, $j = 5, 6, 7, 8$, are not reported for brevity.

4.3 Pulsating flow solution

The solution of the pulsating flow is given by

$$u = u_{\mathrm{s}} + u_{\mathrm{o}} \mathrm{e}^{\mathrm{i}\omega t}, \qquad c = c_{\mathrm{s}} + c_{\mathrm{o}} \mathrm{e}^{\mathrm{i}\omega t},$$

where u_{s}, c_{s} and u_{o}, c_{o} are known from the steady flow and oscillatory flow solutions given in Eqs. (6), (7), (8) and (9), respectively.

4.4 Mass flux

The instantaneous mass flux Q is given by

$$\begin{aligned} Q &= \int_0^1 u_s \,\mathrm{d}y + \left[\int_0^1 u_o \,\mathrm{d}y \right] \mathrm{e}^{\mathrm{i}\omega t}, \\ &= \left(C_1 + \frac{C_2}{\lambda_2}\left(\mathrm{e}^{\lambda_2} - 1\right) + \frac{C_3}{\lambda_3}\left(\mathrm{e}^{\lambda_3} - 1\right) + \frac{C_4}{\lambda_4}\left(\mathrm{e}^{\lambda_4} - 1\right) + \frac{P_{\mathrm{s}}}{2} \right) \\ &\quad + \left(\frac{C_5}{\lambda_5}\left(\mathrm{e}^{\lambda_5} - 1\right) + \frac{C_6}{\lambda_6}\left(\mathrm{e}^{\lambda_6} - 1\right) + \frac{C_7}{\lambda_7}\left(\mathrm{e}^{\lambda_7} - 1\right) + \frac{C_8}{\lambda_8}\left(\mathrm{e}^{\lambda_8} - 1\right) - \frac{\mathrm{i} P_{\mathrm{o}}}{\omega} \right) \mathrm{e}^{\mathrm{i}\omega t}. \end{aligned}$$

4.5 Shear stress

The non-dimensional shear stress at the permeable walls can be obtained from

$$\tilde{\tau} = \frac{\partial u}{\partial y} + mc \quad \text{at } y = 0, 1$$

and the elaborated expression is not reported for brevity.

5 Results and discussion

The analytical solutions for velocity and microrotation profiles for steady, oscillatory and pulsating flows are derived, under the assumption that the lower and upper permeable beds have permeabilities k_1 and k_2, respectively. In the numerical work, we have taken $k_1 = k_2 = k$ (i.e., $\sigma_1 = \sigma_2 = \sigma$).

The effects of various parameters entering into the problem on pulsating velocity $u(y, t)$ are depicted in Figs. 2–4. Fig. 2 shows the variation of the pulsating velocity with respect to t, for $\alpha = 0.5$, $R = 0.5$, $\omega = 1$, $\sigma = 5$, $P_\mathrm{s} = 1$, $P_\mathrm{o} = 1$, $P_j = 1$, $m = 0.5$, $n = 0.5$. At $y = 0$ and $y = 1$, the velocities correspond to the slip velocities at the interfaces of the lower and upper permeable beds, respectively.

In Fig. 3, we see the effect of the microinertia parameter P_j on pulsating velocity profile. As P_j is increasing, the velocity is increasing. From Fig. 4 it is seen that as the parameter σ is increasing, the velocity is decreasing. As $\sigma \to \infty$ (i.e., as $k \to 0$), the velocity corresponds to the pulsating flow between two impermeable plates.

The variation of microrotation with respect to various parameters is shown through Figs. 5–7. From Fig. 5, we see that as ωt is increasing, the microrotation is decreasing near the upper permeable bed while it has an increasing trend at the lower permeable bed. Fig. 6 depicts the variation of microrotation with regard to microinertia parameter P_j. As P_j is increasing, microrotation is decreasing. Fig. 7 shows the variation of microrotation with respect to the parameter σ. As σ is increasing, microrotation is increasing.

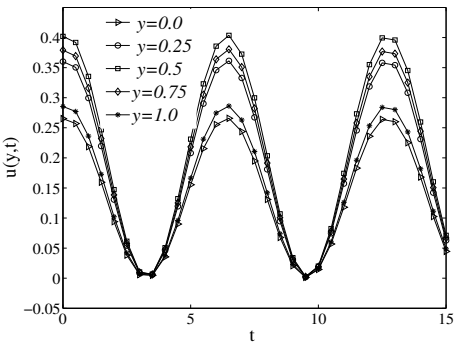

Fig. 2. Variation of $u(y, t)$ for $\alpha = 0.5$, $R = 0.5$, $\omega = 1$, $\sigma = 5$, $P_\mathrm{s} = 1$, $P_j = 1$, $m = 0.5$, $n = 0.5$.

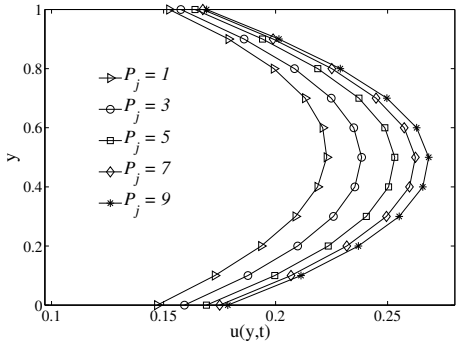

Fig. 3. Effect of P_j on $u(y, t)$ for $\alpha = 0.5$, $R = 0.5$, $\sigma = 5$, $\omega t = \pi/4$, $P_\mathrm{s} = 1$, $P_\mathrm{o} = 1$, $m = 0.5$, $n = 0.5$.

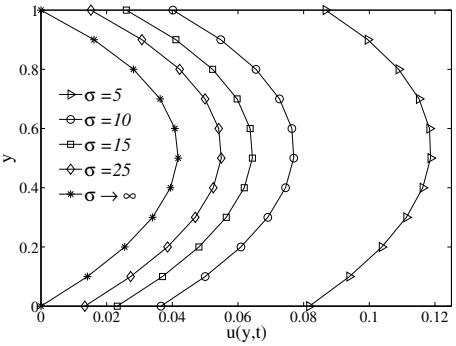

Fig. 4. Effect of σ on $u(y,t)$ for $\alpha = 0.5$, $R = 0.5$, $\omega t = \pi/4$, $P_j = 1$, $P_{\rm s} = 1$, $P_{\rm o} = 1$, $m = 0.5$, $n = 0.5$.

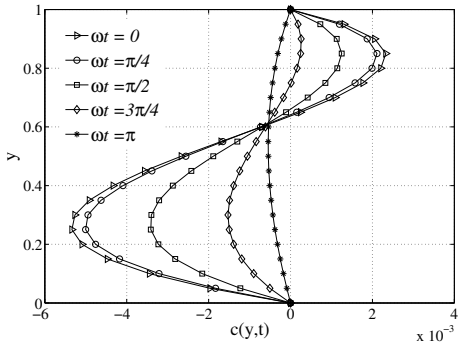

Fig. 5. Effect of ωt on $c(y,t)$ for $\alpha = 0.5$, $R = 0.5$, $\sigma = 5$, $P_{\rm s} = 1$, $P_{\rm o} = 1$, $P_j = 1$, $m = 0.5$, $n = 0.5$.

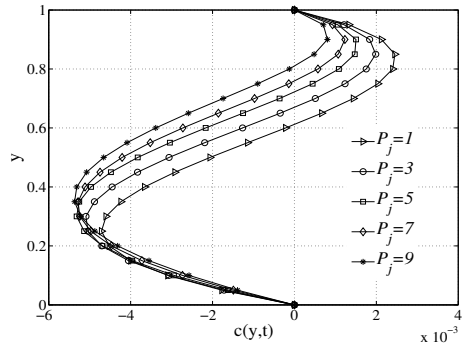

Fig. 6. Effect of P_j on $c(y,t)$ for $\alpha = 0.5$, $R = 0.5$, $\sigma = 5$, $\omega t = \pi/4$, $P_{\rm s} = 1$, $P_{\rm o} = 1$, $m = 0.5$, $n = 0.5$.

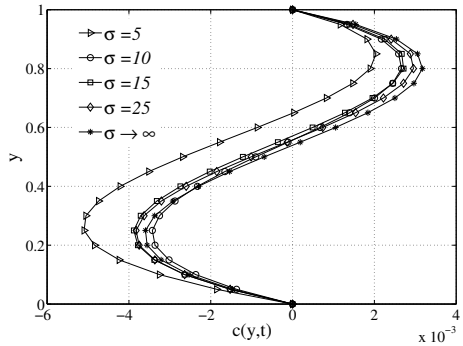

Fig. 7. Effect of σ on $c(y,t)$ for $\alpha = 0.5$, $R = 0.5$, $\omega t = \pi/4$, $P_{\rm s} = 1$, $P_j = 1$, $P_{\rm o} = 1$, $m = 0.5$, $n = 0.5$.

In all Fig. 5–7, the profiles of $c(y,t)$ show a sort of asymmetry about a plane parallel to the beds nearer to the upper bed.

The variation of shear stress τ at the interfaces of the lower permeable bed (LPB) and upper permeable bed (UPB) is presented numerically through Tables 1–6 (with respect to the various parameters entering into the problem). In Table 1, we have presented the variation of shear stress as R increases for a fixed set of values of the other parameters. As the Reynolds number R is increasing through values 1 and 3, at both the permeable beds the shear stress is decreasing and a further increase in R results in an increase in shear stress.

In Table 2, it is seen that as the slip parameter α is increasing for $\omega t = 0$ and $\pi/4$, the shear stress at the LPB is decreasing while it is increasing at the UPB. However, for $\omega t = \pi/2$ and $3\pi/4$ the opposite trend is observed. Table 3 shows that as the parameter σ increases, the shear stress at the LPB decreases, while it shows mixed trend at the UPB

for $\omega t = 0$ and $3\pi/4$. In Table 4, it is seen that for all values of ωt, as the micropolar parameter P_j increases through 0.1 to 0.3, the shear stress increases at both the permeable beds. Further, as P_j increases, the shear stress at the LPB is decreasing while it is increasing at the UPB.

Table 1. Variation of τ with R ($\alpha = 0.1$, $\sigma = 5$, $P_j = 1$, $P_s = 1$, $P_o = 1$, $m = 0.5$, $n = 0.5$).

$\lvert\tilde{\tau}\rvert$		$R = 1$	$R = 3$	$R = 5$	$R = 7$	$R = 9$
$\omega t = 0$	LPB	0.979848	0.1567820	0.4224200	0.43344200	0.3774510
	UPB	1.286140	0.3165710	0.0569092	0.00880363	0.0196955
$\omega t = \pi/4$	LPB	1.082670	0.3830190	0.6816920	0.71707000	0.6836180
	UPB	1.397380	0.0391159	0.2853480	0.37946900	0.4067310
$\omega t = \pi/2$	LPB	0.998402	0.3946530	0.7282030	0.79051200	0.7833660
	UPB	1.309010	0.0098614	0.3745670	0.51661400	0.5879510
$\omega t = 3\pi/4$	LPB	0.776399	0.1848710	0.5347080	0.61074700	0.6182640
	UPB	1.072790	0.2459440	0.1584850	0.32229600	0.4178090

Table 2. Variation of τ with α ($R = 2$, $\sigma = 5$, $P_j = 1$, $P_s = 1$, $P_o = 1$, $m = 0.5$, $n = 0.5$).

$\lvert\tilde{\tau}\rvert$		$\alpha = 0.1$	$\alpha = 0.3$	$\alpha = 0.5$	$\alpha = 0.7$	$\alpha = 0.9$
$\omega t = 0$	LPB	0.936657	0.573655	0.438656	0.374115	0.3362020
	UPB	0.860646	1.118110	1.217080	1.260010	1.2828000
$\omega t = \pi/4$	LPB	0.726260	0.418654	0.348756	0.321073	0.3057420
	UPB	1.104400	1.345180	1.378470	1.377820	1.3710600
$\omega t = \pi/2$	LPB	0.725210	0.623804	0.638052	0.648236	0.6534230
	UPB	1.113570	1.100150	0.996020	0.918140	0.8617010
$\omega t = 3\pi/4$	LPB	0.934124	1.068930	1.137080	1.163960	1.1755800
	UPB	0.882793	0.526551	0.293758	0.150236	0.0531138

Table 3. Variation of τ with σ ($R = 5$, $\alpha = 0.1$, $P_j = 1$, $P_s = 1$, $P_o = 1$, $m = 0.5$, $n = 0.5$).

$\lvert\tilde{\tau}\rvert$		$\sigma = 1$	$\sigma = 3$	$\sigma = 5$	$\sigma = 7$	$\sigma = 9$
$\omega t = 0$	LPB	2.806260	1.237310	0.726009	0.3807060	0.1099640
	UPB	0.706831	0.665932	0.979283	1.1435600	1.2522000
$\omega t = \pi/4$	LPB	2.384920	0.928543	0.419977	0.0876608	0.1593650
	UPB	0.276685	1.019400	1.376730	1.5735300	1.6972700
$\omega t = \pi/2$	LPB	1.646570	0.675970	0.310971	0.0813510	0.0814129
	UPB	0.497893	1.322530	1.545120	1.6362800	1.6615900
$\omega t = 3\pi/4$	LPB	1.023720	0.627548	0.462846	0.3654730	0.2981580
	UPB	1.163170	1.397760	1.385820	1.2950600	1.1660600

Table 4. Variation of τ with P_j ($R = 2$, $\alpha = 0.1$, $\sigma = 5$, $P_{\rm s} = 1$, $P_{\rm o} = 1$, $m = 0.5$, $n = 0.5$.)

$\lvert\tilde{\tau}\rvert$		$P_j = 0.1$	$P_j = 0.3$	$P_j = 0.5$	$P_j = 0.7$	$P_j = 0.9$
$\omega t = 0$	LPB	0.00291110	3.88137	1.81559000	1.183790	0.991881
	UPB	2.16618000	7.21862	0.25079000	0.558923	0.795138
$\omega t = \pi/4$	LPB	0.21326800	4.09173	1.60523000	0.973422	0.781494
	UPB	2.40984000	7.46230	0.00709164	0.802642	1.038880
$\omega t = \pi/2$	LPB	0.21437900	4.09281	1.60417000	0.972367	0.780444
	UPB	2.41899000	7.47144	0.00205461	0.811797	1.048040
$\omega t = 3\pi/4$	LPB	0.00559204	3.88399	1.81302000	1.181250	0.989347
	UPB	2.18825000	7.24069	0.22870900	0.581025	0.817269

Table 5. Variation of τ with m ($R = 5$, $\alpha = 0.1$, $\sigma = 5$, $P_j = 1$, $P_{\rm s} = 1$, $P_{\rm o} = 1$, $n = 0.5$).

$\lvert\tilde{\tau}\rvert$		$m = 0.1$	$m = 0.3$	$m = 0.5$	$m = 0.7$	$m = 0.9$
$\omega t = 0$	LPB	0.904321	0.915776	0.936657	0.9858090	1.232820
	UPB	0.886980	0.878106	0.860646	0.8174890	0.594653
$\omega t = \pi/4$	LPB	0.710028	0.715833	0.726260	0.7505357	0.871701
	UPB	1.112160	1.109890	1.104400	1.0892700	1.006940
$\omega t = \pi/2$	LPB	0.728927	0.727688	0.725210	0.7189880	0.686482
	UPB	1.098390	1.104250	1.113570	1.1333000	1.226130
$\omega t = 3\pi/4$	LPB	0.949946	0.944398	0.934124	0.9096470	0.785660
	UPB	0.853734	0.864495	0.882793	0.9237790	1.123820

Table 6. Variation of τ with n ($R = 5$, $\alpha = 0.1$, $\sigma = 5$, $P_j = 1$, $P_{\rm s} = 1$, $P_{\rm o} = 1$, $m = 0.5$).

$\lvert\tilde{\tau}\rvert$		$n = 0.5$	$n = 1.0$	$n = 1.5$	$n = 2.0$	$n = 2.5$
$\omega t = 0$	LPB	0.726009	0.734893	0.755157	0.795344	0.877727
	UPB	0.979283	0.844418	0.645167	0.327541	0.247911
$\omega t = \pi/4$	LPB	0.419977	0.429278	0.449951	0.490535	0.573306
	UPB	1.376700	1.242280	1.043380	0.726068	0.150888
$\omega t = \pi/2$	LPB	0.310971	0.321078	0.342504	0.383795	0.467231
	UPB	1.545120	1.410470	1.211370	0.893851	0.318462
$\omega t = 3\pi/4$	LPB	0.462846	0.473674	0.495759	0.537651	0.621639
	UPB	1.385820	1.250480	1.050730	0.732606	0.156648

In Table 5, we notice that for $\omega t = 0$ and $\pi/4$, as the coupling parameter m is increasing, the shear stress is increasing at the LPB while it is decreasing at the UPB. This trend is reversed for $\omega t = \pi/2$ and $3\pi/4$. Table 6 shows that at each ωt, as the gyration parameter n is increasing, the shear stress at the LPB is increasing while it is decreasing at the UPB.

6 Conclusions

We have studied the pulsating flow of an incompressible micropolar fluid between permeable beds using Beavers–Joseph slip boundary conditions at the interfaces of the permeable beds. The results reveal that the pulsating velocity of the fluid is reduced by the increase of parameter σ. The presence of microrotation decreases the velocity in comparison with the Newtonian fluid case. As the parameter σ is increasing, the microrotation is decreasing at the LPB while it is increasing at the UPB. Shear stress shows mixed trend with respect to the Reynolds number, slip parameter, parameter σ and microrotation parameter. As the coupling parameter and gyration parameters are increasing, for fixed values of $\omega t = 0, pi/4$, it is seen that the shear stress at the LPB is increasing while it is decreasing at the UPB.

Acknowledgment. We thank the referees for their comments which have resulted in this revised version of the paper.

References

1. D.N. Ku, D.P. Giddens, C.K. Zairns, S. Glagov, Pulsatile flow and atherosclerosis in human carotid bifurcation, *Arteriosclerosis*, **5**:293–302, 1985.

2. R.M. Nerem, M.J. Levesque, Hemodynamics and the arterial wall, in: D.E. Strandness, Jr. et al. (Eds.), *Vascular Diseases: Current Research and Clinical Applications*, Grune and Stratton, Orlando, FL, 1987, pp. 295–317.

3. M.D. Rosello, J.R. Serrano, X. Margot, J.M. Arnau, Analytic-Numerical Approach to Flow Calculation in Intake and Exhaust Systems of Internal Combustion Engines, *Math. Comput. Modelling*, **36**:33–45, 2002.

4. F. Fedele, D. Hitt, R.D. Prabhu, Revisiting the stability of pulsatile pipe flow, *Eur. J. Mech., B, Fluids*, **24**:237–254, 2005.

5. M. Zamir, *The Physics of Pulsatile Flow*, Springer-Verlag, New York, 2000.

6. M.O. Carpinlioglu, M.Y. Gundogdu, A critical review on pulsatile pipe flow studies directing towards future research topics, *Flow Meas. Instrum.*, **12**:163–174, 2001.

7. S. Thomas, S.M. Farouqali, Flow of emulsions in porous media, and potential for enhanced oil recovery, *J. Petrol. Sci. Eng.*, **3**:121–136, 1989.

8. S.T.L. Harrison, M.R. Mackley, A pulsatile flow bioreactor, *Chem. Eng. Sci.*, **47**:490–193, 1992.

9. M. Muskat, *The Flow of Homogeneous Fluids Through Porous Media*, McGraw-Hill, New York, 1937.

10. G.S. Beavers, D.D. Joseph, Boundary conditions at a naturally permeable wall, *J. Fluid Mech.*, **30**:197–207, 1967.

11. D.A. Nield, The Beavers–Joseph boundary condition and related matters: A historical and critical note, *Transp. Porous Med.*, **78**:537–540, 2009.

12. P.D.S. Verma, D.U. Singh, K. Singh, Pulsatile blood flow of a microdeformable fluid, *Wear*, **71**:333–346, 1981.

13. J.C. Misra, S.K. Ghosh, A mathematical model for the study of blood flow through a channel with permeable walls, *Acta Mech.*, **122**:137–153, 1997.

14. K. Vajravelu, K. Ramesh, S. Sreenadh, P.U. Arunachalam, Pulsatile flow between permeable beds, *Int. J. Non-Linear Mech.*, **38**:999–1005, 2003.

15. L. Kumar, S. Narayanan, Analysis of pulsatile flow and its role on particle removal from surfaces, *Chem. Eng. Sci.*, **65**:5582–5587, 2010.

16. A.C. Eringen, Simple microfluids, *Int. J. Eng. Sci.*, **2**:205–217, 1964.

17. A.C. Eringen, Theory of micropolar fluids, *J. Math. Mech.*, **16**:1–18, 1966.

18. A.C. Eringen, *Microcontinuum Field Theories II: Fluent Media*, Springer-Verlag, New York, 1998.

19. G. Lukaszewicz, *Micropolar Fluids: Theory and Applications*, Birkhauser, Boston, 1999.